Design and Performance of the Hyper-Cam, an Infrared Hyperspectral Imaging Sensor

Philippe Lagueux[*a], Vincent Farley[a], Martin Chamberland[a], André Villemaire[a] ,
and Caroline Turcotte[b], Eldon Puckrin[b]
[a]Telops inc., 100-2600 St-Jean-Baptiste, Québec, Qc, Canada G2E 6J5
[b]Defence R&D Canada – Valcartier, 2459 Pie-XI Blvd N., Québec, QC, Canada G3J 1X5

1. Introduction

Emerging applications in Defense and Security require sensors with state-of-the-art sensitivity and capabilities. Among these sensors, the imaging spectrometer is an instrument yielding a large amount of rich information about the measured scene. This powerful spectrometric tool is becoming more common in civil applications such as search and rescue, geological surveys, pollution monitoring, forest fire detection and monitoring and combustion studies. These sensors are now also emerging as indispensable assets for defence operations through the role they can play for troop protection against chemical attacks, detection of mines and unexploded ordnance (UXO) and for the detection of camouflaged targets. Imaging spectrometers have unmatched capabilities to meet the requirements of these applications.

Telops has developed the Hyper-Cam LW and Hyper-Cam MW hyperspectral imagers. The former operates in the 8-12 µm longwave infrared (LWIR) spectral range and the latter in the 3-5 µm midwave infrared (MWIR) spectral range, with an extendable option to shorter wavelength. The Hyper-Cam is based on the Fourier-transform technology yielding high spectral resolution and enabling high-accuracy radiometric calibration. The Hyper-Cam, a portable sensor, provides datacubes of up to 320x256 pixels at 0.35 mrad spatial resolution and at spectral resolutions of up to 0.25cm^{-1}. The Hyper-Cam LW has been used in several ground-based field campaigns, including the demonstration of standoff chemical agent detection [1].

More recently, the Hyper-Cam has been integrated into an airplane to provide airborne measurement capabilities. A special pointing module was designed to compensate for airplane attitude and forward motion. To our knowledge, the Hyper-Cam is the first commercial airborne hyperspectral imaging sensor based on Fourier-transform infrared technology.

The Hyper-Cam sensor is described in section 2 and the airborne sensor is presented in section 3. Sections 4 and 5 respectively present the spatial and spectral resolution of the Hyper-Cam. In section 6, the sensitivity of the sensor is described in terms of NESR. The accuracy and stability of the radiometric data acquired, two primordial characteristics reported in section 7, prove the unmatched performance of the Hyper-Cam. Finally, the unparalleled capabilities of the FIRST for standoff chemical detection (ground and airborne) are exposed in section 8.

2. Description of the Hyper-Cam Sensor

The Hyper-Cam sensor is a lightweight and compact imaging spectroradiometer. The spectral measurements are performed using a Fourier-Transform Spectrometer (FTS). It uses a 320x256 LWIR PV-MCT focal plane array detector that can be windowed and formatted to fit the desired size and to decrease the acquisition time. Spectral resolution is user-selectable from 0.25 to 150 cm^{-1}. This instrument measures the complete spectrum of each pixel in the image, each pixel having an instantaneous field-of-view of 0.35 mrad. The latest version of this field-portable sensor is shown in Figure 1. This version is conduction-cooled and sealed from the environment. It is thus ideally designed to withstand operation in harsh and dusty conditions.

Figure 1: Photograph of the Hyper-Cam

[*] philippe.lagueux@telops.com; phone (418) 864-7808; fax (418) 864-7843; www.telops.com

Report Documentation Page

Public reporting burden for the collection of information is estimated to average 1 hour per response, including the time for reviewing instructions, searching existing data sources, gathering and maintaining the data needed, and completing and reviewing the collection of information. Send comments regarding this burden estimate or any other aspect of this collection of information, including suggestions for reducing this burden, to Washington Headquarters Services, Directorate for Information Operations and Reports, 1215 Jefferson Davis Highway, Suite 1204, Arlington VA 22202-4302. Respondents should be aware that notwithstanding any other provision of law, no person shall be subject to a penalty for failing to comply with a collection of information if it does not display a currently valid OMB control number.

1. REPORT DATE **OCT 2009**	2. REPORT TYPE **N/A**	3. DATES COVERED **-**

4. TITLE AND SUBTITLE **Design and Performance of the Hyper-Cam, and Infrared Hyperspectral Imaging Sensor**	5a. CONTRACT NUMBER
	5b. GRANT NUMBER
	5c. PROGRAM ELEMENT NUMBER
6. AUTHOR(S)	5d. PROJECT NUMBER
	5e. TASK NUMBER
	5f. WORK UNIT NUMBER
7. PERFORMING ORGANIZATION NAME(S) AND ADDRESS(ES) **Telops inc. Quebec, QC, Canada**	8. PERFORMING ORGANIZATION REPORT NUMBER
9. SPONSORING/MONITORING AGENCY NAME(S) AND ADDRESS(ES)	10. SPONSOR/MONITOR'S ACRONYM(S)
	11. SPONSOR/MONITOR'S REPORT NUMBER(S)

12. DISTRIBUTION/AVAILABILITY STATEMENT
Approved for public release, distribution unlimited

13. SUPPLEMENTARY NOTES
See also ADB381583. RTO-MP-SET-151 Thermal Hyperspectral Imagery (Imagerie hyperspectrale thermique). Meeting Proceedings of Sensors and Electronics Panel (SET) Specialists Meeting held at the Belgian Royal Military Academy, Brussels, Belgium on 26-27 October 2009., The original document contains color images.

14. ABSTRACT

15. SUBJECT TERMS

16. SECURITY CLASSIFICATION OF:			17. LIMITATION OF ABSTRACT **SAR**	18. NUMBER OF PAGES **12**	19a. NAME OF RESPONSIBLE PERSON
a. REPORT **unclassified**	b. ABSTRACT **unclassified**	c. THIS PAGE **unclassified**			

The instrument features 2 internal calibration blackbodies used to perform a complete end-to-end radiometric calibration of the measurements (see Section 5). In its longwave IR version, the instrument has good sensitivity over the 8-12 µm band. This spectral band is ideal for standoff chemical agent detection at ambient temperatures. The sensor also has acquisition and processing electronics, including 4 GB of high-speed DDR-SDRAM, with the capability to convert the raw interferograms into spectra using real-time Discrete-Fourier Transform (DFT).

The instrument outputs the measurements on a high-speed CameraLink interface. The configuration, monitoring and real-time housekeeping data collection is performed using an Ethernet link. A bore-sight video camera takes simultaneous visible images aligned with the imaging FTS. The instrument supports two operating modes: FTS mode and Camera mode. In Camera mode, the instrument generates a standard broadband thermal IR digital video and supports up to 300 frames per second with the full 320 x 256 pixels of the focal plane array area. In FTS mode, the interferograms or the spectra are transferred along with a header containing all configuration parameters and monitored values to be stored on the computer.
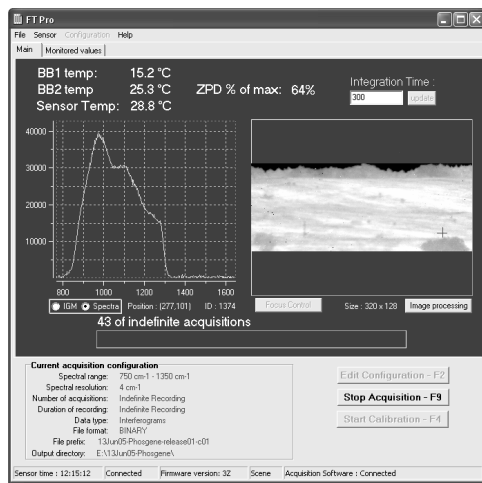

Figure 2: FTPro™ control software

The FTPro™ control software provides a user-friendly interface, giving real-time feedback to the operator. A screenshot of the control software is presented in Figure 2 on the left-hand side. On the right panel, the non-uniformity corrected broadband IR image is displayed in grayscale where black corresponds to low radiance level and white corresponds to high radiance level. The uncalibrated raw spectrum (or the interferogram as selected by the operator) of a selected pixel in the image is displayed in real time on the left of the screen. Additional key parameters such as the blackbodies temperature, the sensor temperature and the level of signal on the FPA are also displayed. Additional monitored values can be viewed in a separate panel. This main panel of the user interface is used to start the acquisition of the data or to initiate calibration measurements. The configuration of the sensor (image size and location, spectral resolution, blackbody and sensor temperatures, etc…) is performed with another input panel. The integration time of the FPA can be changed from the main panel.

The sensor has the capability to change the focus of the IR image to produce a clear image at any distance from 2 meters up to infinity. The Hyper-Cam was presented in detail in previous papers [4, 5, 6 and 7].

3. Airborne configuration

The Hyper-Cam airborne system comprises the Hyper-Cam instrument along with several modules. The primary function of the assembly is to compensate for the aircraft displacement and its angular pitch, roll and yaw. It also adds accurate aircraft position and attitude data to the acquisition file metadata in order to later geo-reference the acquired data. The following section describes the role of each subsystem to fulfill the flight requirements.

In order to acquire the most useful infrared spectral ranges, the Telops airborne system allows mounting two different Hyper-Cam instruments. The Hyper-Cam MW measures from 3 to 5.5 µm whereas the Hyper-Cam LW measures the 8 to 11.5 µm wavelength range. The optical bench includes a stabilization platform, the two Hyper-Cam instruments, two IMC mirrors, a GPS/INS unit and two visible boresight cameras. All these modules are rigidly mounted on a high-stiffness base plate. This base plate is mounted on the stabilization platform. Figure 3 illustrate the Hyper-Cam airborne configuration.
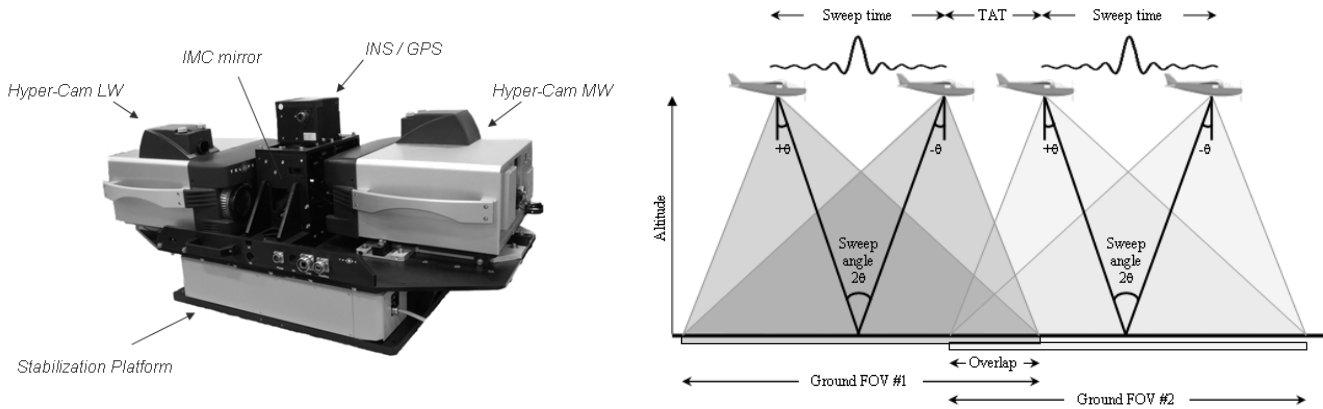
Figure 3. Illustration of the airborne configuration with two Hyper-Cams

The IMC mirrors are used to compensate the airplane pitch, roll and forward motion (independently for each Hyper-Cam sensor), while the stabilization platform is used to dampen the airplane vibrations and to compensate the airplane yaw. The IMC mirrors are controlled by the navigation module which receives and uses the information from two video trackers (one from each Hyper-Cam) and a GPS/INS unit. The GPS/INS also enables ortho-rectification and geo-referencing of the collected data.

The Hyper-Cam instruments offer uncommon flexibility in adjusting their spatial, spectral and temporal parameters. This flexibility proves to be invaluable for airborne applications where the flight parameters impose severe restrictions on spectrometer operation. Additional details on the Hyper-Cam airborne system design are provided in [3].

4. Spatial Resolution

To produce a high-quality IR image of the scene, Telops designed the optical assembly such that the blur is smaller than the diffraction from this f/2 system. With the FPA's 30 µm pixels and the lens focal length of 86 mm, a 0.35 mrad IFOV is obtained. The lens produces a pupil image in the interferometer (close to the corner cube) in order to minimize vignetting and maintain high sensitivity without increasing the size of the interferometer. To maintain the high image quality notwithstanding temperature variations, Telops implemented a servo-controlled autofocus. This efficient system allows maintaining the diffraction limited performance over a wide range of temperatures. Figure 4 presents a picture of the lens assembly.
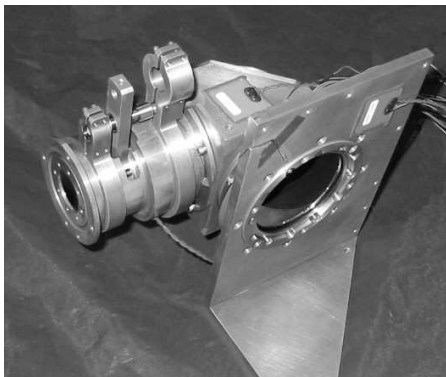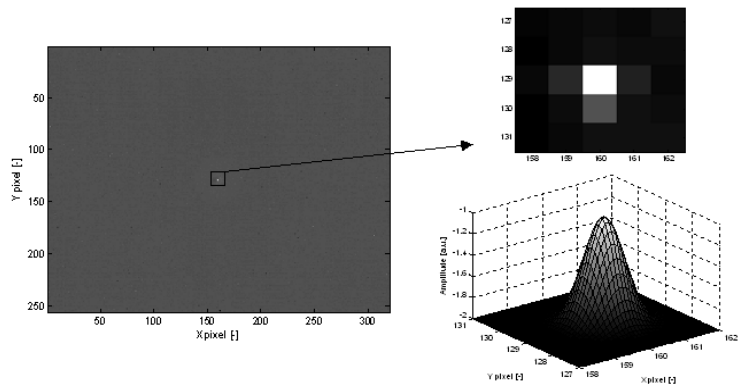
Figure 4: IR lens photograph

Figure 5: Measured optical blur for a collimated source in the center of the FOV

The optical blur of the system was measured by looking at a collimated hot source. The divergence of the hot source was 78 µrad, i.e. less than ¼ of a detector pixel. Figure 5 shows the blur spot at the center of the FOV.

Table 1 gives the measured optical blur for different locations in the field-of-view. The optical blur FWHM is of the same order of magnitude as the pixel IFOV (350 µrad), and the autofocus allows achieving this performance for a wide range of temperatures exceeding 0 to 50°C.

TABLE 1 : Optical blur measurements

POSITION IN FOV	BLUR FWHM [µrad]
CENTER	386
TOP-LEFT CORNER	386
TOP-RIGHT CORNER	486
BOTTOM-LEFT CORNER	426
BOTTOM-RIGHT CORNER	419

5. Spectral Resolution

Spectral resolution represents the capacity of a sensor to resolve two adjacent frequencies. This parameter is thus one of the most important characteristic of any spectrometer especially for applications that require a narrow spectral resolution and a good spectral accuracy.

To test the spectral response of a spectrometer, a spectral impulse is measured by the sensor and the line broadening is analyzed. In order to do so, an adequate spectral target needs to be identified. The target must exhibit at least one very narrow and strong spectral line. Of course, the position of the spectral line must also be accurately known. Water vapor possesses spectral features in the LWIR region of the electromagnetic spectrum, within the spectral range of the Hyper-Cam LW. On a cloudless day, the deep sky offers a background with good thermal contrast for the measurement of the spectrum of atmospheric water vapor. Figure 6 shows the calibrated spectrum of a deep sky measurement. For this test, nine cubes of 320x256 pixels were co-added and the spectral resolution was set to 0.25 cm^{-1}. Water vapor emission lines are seen in the 1100 to 1250 cm^{-1} region. Also, ozone emission is seen in the 1000 to 1075 cm^{-1} region.
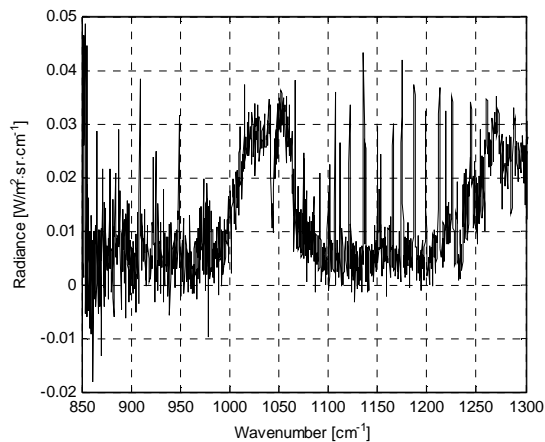

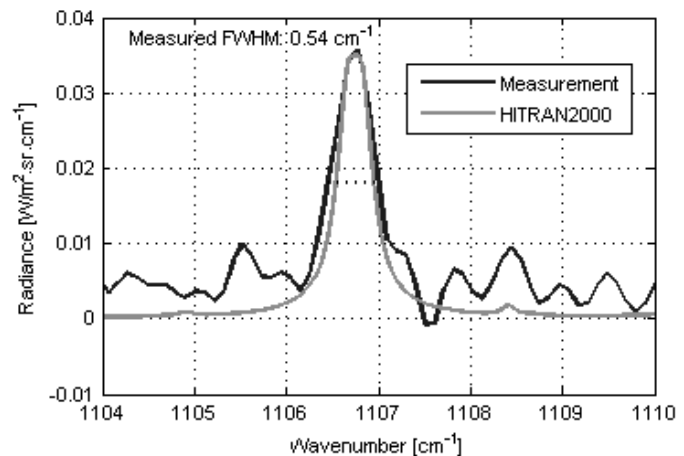Figure 6: Deep sky calibrated measurement of the center pixel with 0.25 cm^{-1} spectral resolution

Figure 7: Zoom on the water vapor emission line at 1106.745 cm^{-1}

MOLSPECT with HITRAN2000 database was used to compare the experimental results with theory. The parameters indicated in Table 2 were used to generate the data. A simplified model of the atmosphere is assumed, using a single layer of gas. It was determined that an appropriate spectral line to determine the spectral resolution of the Hyper-Cam LW is situated at 1106.745 cm^{-1}.

TABLE 2 : Assumed conditions to generate the atmospheric spectrum with HITRAN2000

Atmsopheric condition	Value	Unit
Relative humidity	50	%
Water vapor partial pressure	8.77	mm Hg
Depth of gas sample	1	km
Gas temperature	20	°C
Atmospheric pressure	1	atm

On Figure 7, the measured spectrum is superimposed on the normalized HITRAN2000 spectral signature near the above-mentioned line. The FWHM of the measured emission line is 0.54 cm^{-1}. However, the width of the atmospheric water vapor line strongly depends on the atmospheric conditions (vertical temperature and humidity profiles). The expected width can lie anywhere between 0.3 and 0.7 cm^{-1}, so by getting a measurement of 0.54, we can conclude that the Hyper-Cam resolution is better than 0.5 cm^{-1}. By design, the expected spectral resolution is 0.25 cm^{-1}, and another experiment setup is needed to measure it.

6. NESR

The sensitivity of infrared hyperspectral sensors based on Fourier transform spectrometers is generally specified in Noise Equivalent Spectral Radiance (NESR). Our NESR model was used to predict the performance of the Hyper-Cam hyperspectral sensor. Measurements performed in a field campaign allowed to validate the model experimentally.

In order to evaluate the NESR from experimental data, a two-point radiometric calibration technique, described in detail in [2], is implemented. Two sets of blackbody measurements – one with a cold blackbody and one with a hot blackbody – are required. These measurements enable to calculate the sensor gain and offset which are used to perform the radiometric calibration (as explained in [1]).

Next, a sequence of scene measurements is acquired, with a blackbody positioned in the sensor field-of-view. This represents the ideal scene to measure the NESR, as the temporal variations of the scene radiance are negligible with a well controlled blackbody. Thus, the NESR is evaluated spectrally by calculating the temporal standard deviation of the measured radiance for each measured spectral bin.

The NESR measurement was performed for each pixel in the 128x128 central zone of the detector. Next, the bad pixels were eliminated from the group, and the remaining 97% of the pixels were averaged to give the measured spectral NESR shown in Figure 8.
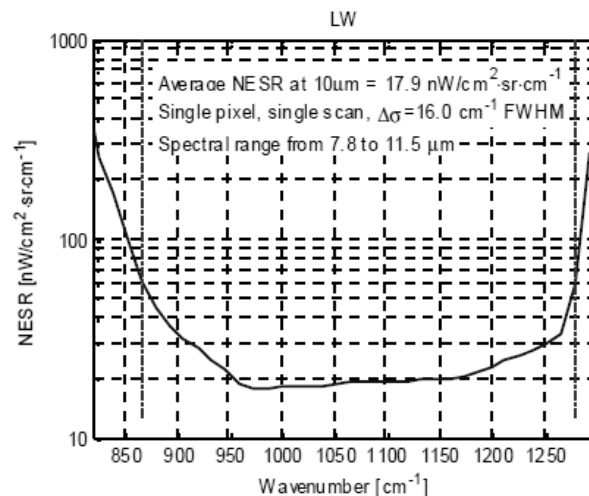

Figure 8: Measured and predicted Hyper-Cam sensor spectral NESR.

Note that the general NESR increase around 850 cm^{-1} is due to the detector cut-off, while the NESR increase above 1280 cm^{-1} is due to the optical cold filer in front of the focal plane array. The discrepancy observed between the predicted and experimental NESR between 950 and 1250 cm^{-1} is around 20%. Note that some parameters used in the model are known with an accuracy of ~20%, and thus, the agreement obtained between the predicted and measured NESR is satisfactory.

7. Radiometric Accuracy and Stability

The radiometric calibration of FTIR instruments used for remote sensing was developed and refined in the late 1980s [1]. The result of this work yielded a simple and powerful calibration approach that corrects for instrument response, accurately removes the instrument self-emission and corrects for phase characteristics of the FTIR.

Radiometric calibration basically consists in characterizing the FTS response by a linear expression, i.e. by a gain (or slope) and an offset. The gain and offset are characterized as a function of the wavelength, and they are complex to represent the phase of the FTS as well. These gain and offset include the response of the interferometer, of the detector and of the associated electronics. Thus, the linearity of the detector and associated electronics is important. This concept is explained in detail in a previous paper [2]. From the information obtained in the calibration process, one can study the absolute radiance accuracy and the radiometric accuracy.

The absolute radiance accuracy of a remote sensing instrument is one of its fundamental characteristics. Physical parameters derived from field spectra are directly affected by the ability of the sensor to produce measurements with good radiometric fidelity.

The stability of the radiance accuracy over time, often referred to as the radiometric stability, is equally important. It dictates the frequency at which the radiometric calibration process needs to be performed. In this paper, a large quantity of experimental calibration data acquired during two field campaigns in the summer of 2005 is used to analyze the radiometric stability of Telops' Hyper-Cam sensor. This study has the flavor of similar studies that were performed on other FTIR sensors, e.g. the study of the DRDC Valcartier CATSI radiometric stability presented in [3].

7.1. Radiometric Accuracy

The radiometric accuracy was measured by comparing the calibrated spectrum measurement of an external blackbody with its theoretical radiance. The comparison is made in brightness temperature units. The external blackbody temperature was set to 30°C.

Figure 9 shows the spectral radiometric accuracy in Kelvin. It is better than 0.5 K over the spectral range of the sensor.
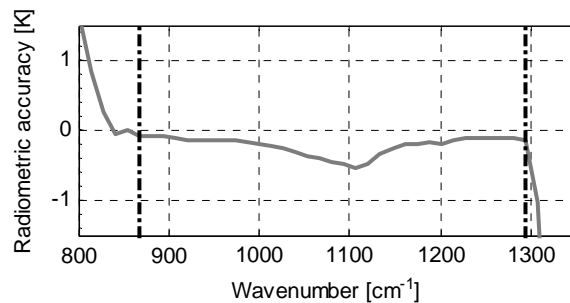

Figure 9: Spectral radiometric accuracy measurement

7.2. Experimental Data for Radiometric Stability Analysis

The Hyper-Cam sensor was used in two major field campaigns in the summer of 2005. First, it was used in a four-week campaign in England in June 2005. This trial was held at DSTL in Porton Down. Telops staff operated the Hyper-Cam sensor during this campaign aimed at testing standoff gas detection with remote sensors. The gas detection results are presented in section 8 and in more details in [7]. A photograph of the sensor at the Porton Down trial is shown in Figure 10.

Second, the Hyper-Cam sensor was used in a two-week field campaign in Utah in July 2005. This trial was held at Dugway Proving Grounds near Salt Lake City. Staff from the Johns Hopkins University Applied Physics Laboratory operated the loaned Telops' FIRST sensor in this campaign. They shared their calibration data with Telops for the purpose of this study.

The calibration data acquired during these two field campaigns was analyzed in order to study the Hyper-Cam radiometric stability. 120 radiometric calibrations were performed during the Porton Down trial, and 41 radiometric calibrations were performed during the Dugway campaign. Thus, the experimental data consists in a total of 161 radiometric calibrations acquired in two different continents over a 2-month time interval.

Figure 10: Hyper-Cam sensor at the DSTL
campaign in Porton Down, UK

All the results presented in this paper are based on this data. Figure 11 shows the ambient temperature and the sensor temperature (measured on the modulator) over the entire time of the field campaigns. The ambient temperature varied between 15 and 33°C, and the sensor temperature varied between 18 and 42°C. Note that the zero time reference is 7 June 2005 at midnight.
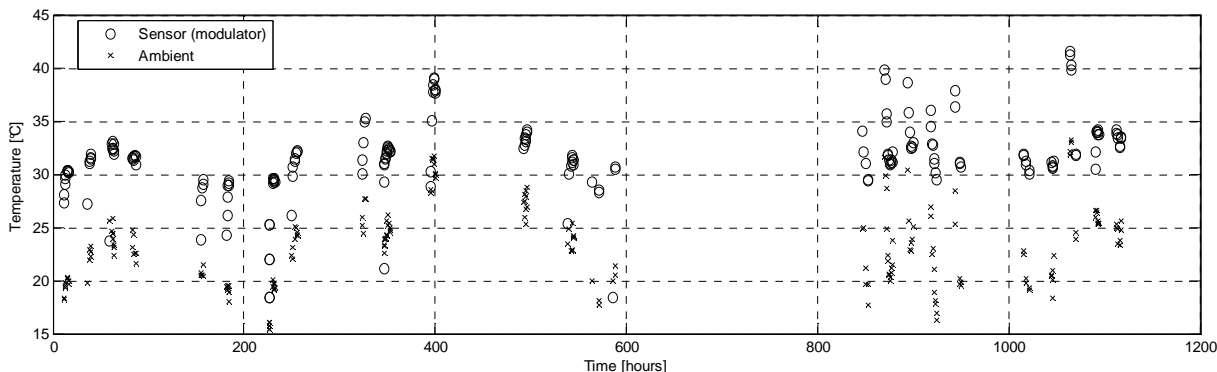

Figure 11: Ambient and sensor temperatures during the field campaigns. Seemingly vertical groups represent the usual daily temperature increase or nocturnal decrease.

The sensor was operated with fixed parameters during the two campaigns. The parameters are a centered spatial window of 320×128 pixels, a spectral resolution of 4 cm^{-1}, a focus adjustment at infinity and blackbody temperatures adjusted to approximately 5 degrees Celsius below and above ambient temperature (for the cold and hot reference targets).

Note that during the two field campaigns, the Hyper-Cam sensor was used without taking advantage of its sensor temperature stabilization feature. This feature consists in heaters that are strategically positioned on the sensor key parts; i.e. the interferometer and the lens mechanical assemblies. These heaters can be used to maintain the instrument temperature stable regardless of the ambient temperature fluctuations. By disabling this feature, the data acquired allowed to evaluate the radiometric stability as a function of the instrument temperature fluctuations.

7.3. Experimental Radiometric Calibration Stability Analysis

Figure 12 shows the magnitude and phase of the gain averaged over all the good pixels, for all the 161 radiometric calibrations of the two field campaigns. The gain magnitude decrease in the 850 cm^{-1} region is caused by the detector cut-off, while the gain decrease around 1300 cm^{-1} is due to the presence of an optical cold filter in front of the detector. The spectral shape in this data shows that there is a significant advantage to characterize the gain as a function of the wavelength, as a lot of spectral variations are not considered if only a broadband calibration is performed. This illustrates an advantage that a spectral sensor has over a broadband sensor to achieve accurate radiometry.

The result from Figure 12 indicates that the spectral shape of the gain magnitude has not changed significantly during the entire time lapse. Given this observation, the analysis of the gain magnitude simply considers the fluctuations that are observed on the spectral average of the gain magnitude, between 900 and 1250 cm^{-1}.

Figure 12: Measurements of the magnitude and phase of the gain, averaged for all pixels

Also, the results for all the good pixels are averaged together in order to reduce the noise level. "Bad" pixels - roughly 3% of the 40,960 pixels of the 320×128 window that was used in the field campaigns - are excluded from this averaging.

Figure 13 shows the magnitude of the offset of all the calibration measurements, averaged for all the good pixels, in units of brightness temperature. The phase of the offset is also shown. The offset of all pixels is very similar to the radiance spectrum of a cold blackbody. This is because the sensor has a good transmittance, and thus a low radiometric offset. Furthermore, since the instrument is in a 2-port configuration, the contribution of the output port to the radiometric offset is very low, as the detector is cooled down to 68 K.

The offset is very low (~215 K), which indicates that the shot noise coming from the instrument radiance is minimized. This helps to reduce the noise level, since the FIRST is shot noise limited.

Figure 13: Magnitude of the offset in brightness temperature, averaged for all pixels

The detailed analysis of the radiometric stability was presented in [2]. The result indicates a total radiance accuracy of 1.8% ($\sqrt{1.6\%^2 + 0.6\%^2 + 0.6\%^2}$). We emphasize that this level of accuracy is obtained with simple temperature compensation and without recalibrating the instrument by measuring calibration blackbodies. It is also implied that a phase correction is performed when the sensor is turned off and back on. The radiometric accuracy obtained right after a calibration is presented on Figure 9.
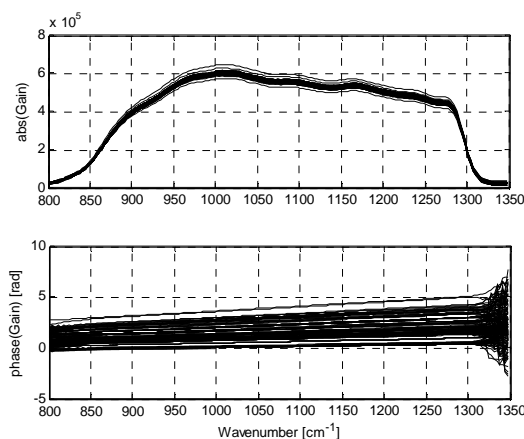
8. Hyper-CAM as a Standoff Chemical Detector

Several chemicals, including some mixtures, were released during the field test conducted in England in June 2005. The Hyper-Cam, combined with gas detection algorithms developed by Telops, was capable of detecting and identifying the various chemicals released [7]. Since the Hyper-Cam also gives temporal information, we are able to produce videos of chemicals clouds as they disseminate. The measurement rate of the Hyper-Cam depends on the image size and spectral resolution. When used at 4 cm^{-1} of spectral resolution with an image size of 320×128, the measurement rate is approximately 1 datacube every 4 seconds. This is enough to see continuous gas cloud displacement. Figure 14 presents typical examples of gas detection measurements. They present the broadband IR image in background with an overlay of the chemicals detected and identified. The overlay has a variable transparency. Where the scores of 2 different criteria are above the thresholds, the transparency is displayed and it is proportional to the score of a clutter-matched filter calculation. This gives an indication of the concentration of the chemical and this also displays clearly the cloud shape. Telops' web site (www.telops.com) has video files from Hyper-Cam measurements that can be downloaded and played. They give a very good feeling of the powerful standoff chemical agent detection and identification capability of the Hyper-Cam.
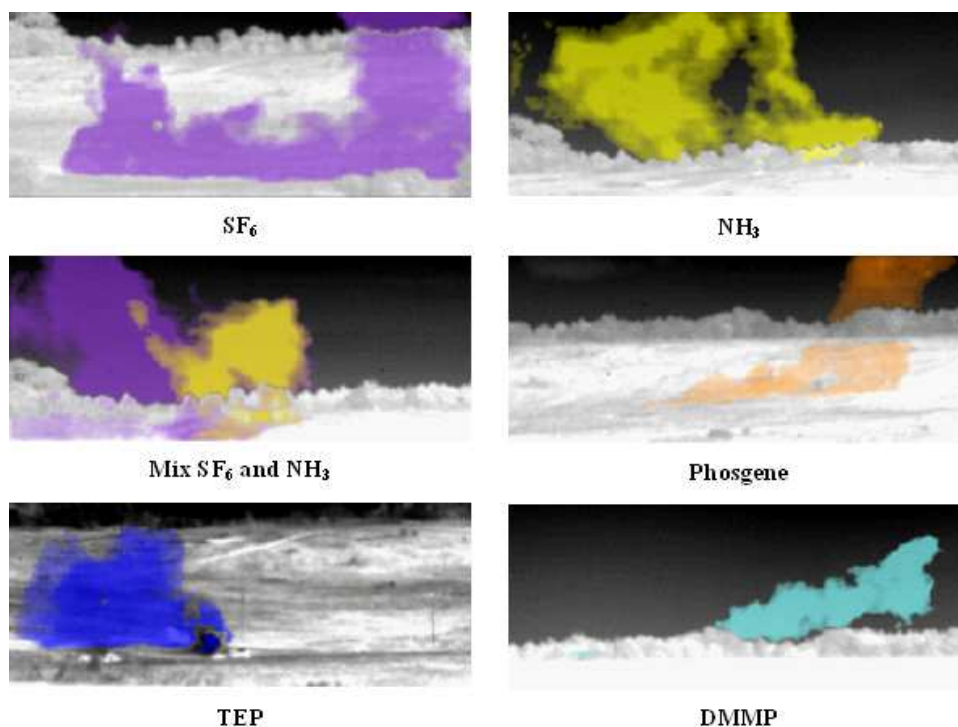

Figure 14. Typical results of chemical detection obtained with the FIRST

9. Airborne chemical detection using the Hyper-CAM

An experiment was set up at DRDC Valcartier to test the capability of the airborne Hyper-Cam-LW sensor for detecting gas plumes, plastic 'plumes', and chemical powders, along with a number of calibration panels to help quantify the noise equivalent spectral radiance (NESR) and sensor pointing stability. The DRDC experiment was carried out on December 19, 2008. The experiment was set up under cold, clear sky conditions; unfortunately, overcast cloud cover formed by the time the aircraft was ready to acquire data. A second experiment was carried out on March 25, 2009 in which the airborne Hyper-Cam was able to acquire measurements over a Canadian industrial site under clear sky conditions. The two experiments and their results are summarized in the next sub-sections.
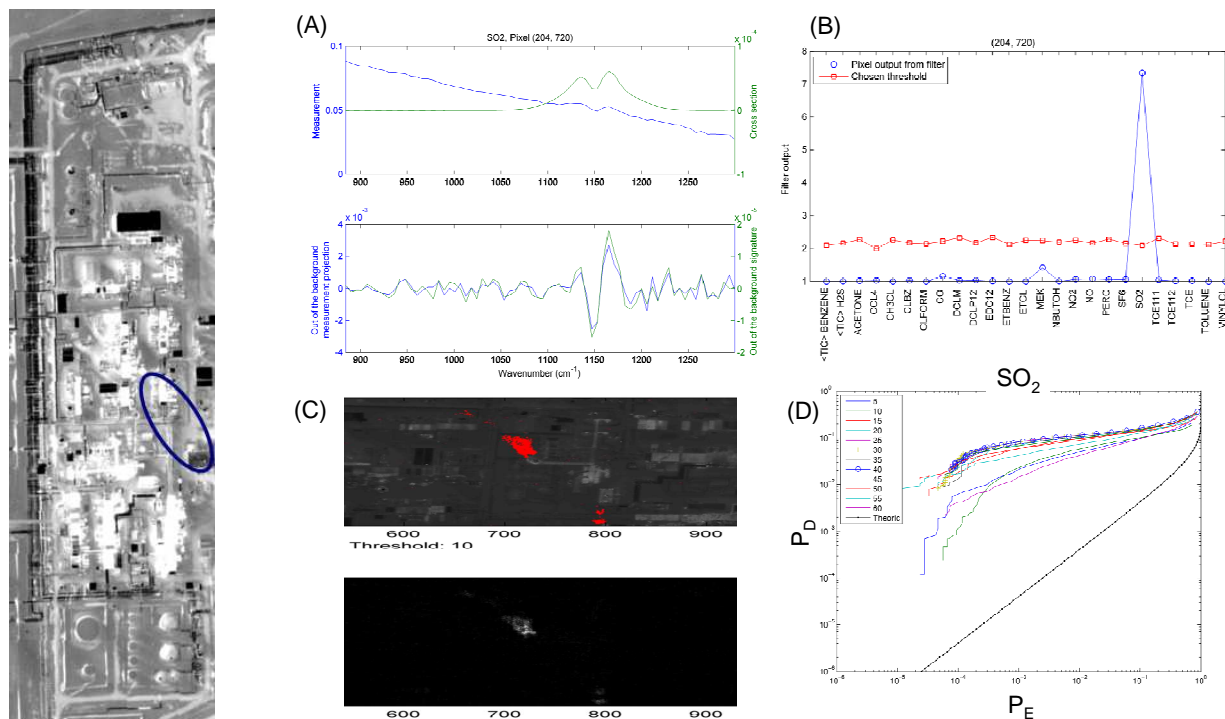
Figure 15. The detection and identification of SO_2 gas at the industrial site using the GLRT algorithm. (A) Measured radiance and SO_2 signature (upper panel), and projected measurement and SO_2 signature results (lower panel). (B) Filter output showing the clear detection and identification of SO_2 well above the threshold value. (C) Identification of the plume in the LWIR image. (D) ROC curves for SO_2 for a different numbers of basis vectors.

10. Conclusion

Telops has developed a powerful and versatile imaging spectrometer. The Hyper-Cam, operating in the LWIR band, is well suited for standoff chemical agent detection and can be used as a powerful hyperspectral imager for any scientific application. Excellent spectral resolution coupled to a high sensitivity are used to identify the chemical agents and discriminate interferents. The spatial and temporal resolutions allow the detailed tracking of gas cloud evolution that should provide invaluable information to the chemical cloud dispersion modeling community.

It was shown in this paper that over a period of 40 days, the radiance accuracy of the Hyper-Cam sensor remains better than 2%, with a single radiometric calibration. This assumes that the sensor temperature is stabilized, or that a linear correction based on the instrument temperature is applied on the gain phase and offset magnitude. This also implies that a phase correction is performed when the sensor is turned off and back on. This radiometric stability measured in the field underlines the quality of the Hyper-Cam sensor.

It was also shown in this paper that a simple spectral calibration of the Hyper-Cam sensor ensures a spectral accuracy of $0.3\ cm^{-1}$ for each pixel, when using a $0.5\ cm^{-1}$ spectral resolution. This assumes that a simple correction for the instrument lineshape is performed. The stability of the spectral calibration over time will be characterized in future tests.

REFERENCES

[1] H.E. Revercomb, H. Buijs, H.B. Howell, D.D. Laporte, W.L. Smith, and L.A. Sromovsky, *Radiometric calibration of IR Fourier transform spectrometers: Solution to a problem with the high-resolution interferometer sounder*; Applied Optics, vol. 27, issue 15, pp. 3210-3218, August 1988.

[2] Vincent Farley, Martin Chamberland, Alexandre Vallières, André Villemaire and Jean-François Legault, *Radiometric Calibration Stability of the FIRST : a Longwave Infrared Hyperspectral Imaging Sensor*, Proc. SPIE Vol. 6206, Infrared Technology and Applications XXXII;

[3] A. Villemaire, M. Chamberland, J. Giroux, R. L. Lachance, J.-M. Thériault, *Radiometric calibration of FT-IR remote sensing instrument*; Proc. SPIE Vol. 3082, pp. 83-91, Electro-Optical Technology for Remote Chemical Detection and Identification II; Mahmoud Fallahi, Ellen A. Howden; Eds., July 1997.

[4] M. Chamberland et al., *Advancements in field-portable imaging radiometric spectrometer technology for chemical detection,* Proc. SPIE Vol. 5416, pp. 63-72, Chemical and Biological Sensing V; Patrick J. Gardner; Ed., August 2004.

[5] V. Farley et al., *Development and testing of a hyper-spectral imaging instrument for field spectroscopy,* Proc. SPIE Vol. 5546, pp. 29-36, Imaging Spectrometry X; Sylvia S. Shen, Paul E. Lewis; Eds., October 2004.

[6] M. Chamberland et al., *Development and testing of a hyper-spectral imaging instrument for standoff chemical detection*, Proc. SPIE Vol. 5584, pp. 135-143, Chemical and Biological Standoff Detection II; James O. Jensen, Jean-Marc Theriault; Eds., December 2004.

[7] A. Vallières et al., *High-Performance Field-Portable Imaging Radiometric Spectrometer Technology For Chemical Agent Detection*, Proc. SPIE Vol. 5590, pp. 211-219, Optically Based Materials and Optically Based Biological and Chemical Sensing for Defence II; John C. Carrano, Arturas Zukauskas, Anthony W. Vere, James G. Grote, François Kajzar; Eds., October 2005.

[8] C. A. Klein, R. P. Miller, and D. L. Stierwalt, *Surface and bulk absorption characteristics of chemically vapor-deposited zinc selenide in the infrared*, Applied Optics, vol. 33, issue 19, pp. 4304-4313, 1994.